Phantom and clinical evaluation of a new Bayesian penalized likelihood reconstruction algorithm HYPER Iterative on the image quality of 68Ga-DOTA-NOC PET/CT

Lei Xu (xulei09060118@163.com)
Nanjing First Hospital
Can Cui
Jiangsu Cancer Hospital
Rushuai Li
Nanjing First Hospital
Rui Yang
Nanjing First Hospital
Rencong Liu
Nanjing First Hospital
Qingle Meng
Nanjing First Hospital
Feng Wang
Nanjing First Hospital

Research Article

Keywords: PET, 68Ga-DOTA-NOC, Neuroendocrine neoplasm, Image reconstruction, Bayesian penalized likelihood, Penalization factor

Posted Date: August 3rd, 2022

DOI: https://doi.org/10.21203/rs.3.rs-1310776/v1

Abstract

Background

Bayesian penalized likelihood (BPL) algorithm is an effective way to suppress the noise by incorporating a smooth penalty in the positron emission tomography (PET) image reconstruction process. The strength of the smooth penalty is controlled by the penalization factor. The aim was to investigate the impact of different penalization factor and acquisition time in a new BPL algorithm HYPER Iterative on the image quality of ^{68}Ga-DOTA-NOC PET/CT. A phantom and 25 patients with neuroendocrine neoplasm underwent ^{68}Ga-DOTA-NOC PET/CT were included. The PET data were acquired with a digital PET/CT in a list-mode and reconstructed by ordered subset expectation maximization (OSEM) and HYPER Iterative algorithm with seven penalization factors between 0.03 and 0.5 for 2 and 3 minutes-per-bed (m/b) acquisition, both including time of flight and point of spread function recovery. The contrast recovery (CR) and background variability (BV) of the phantom, SUV_{mean} and coefficient of variation of liver (CV), and SUV_{max} of the lesions were measured. Image quality was ranked by two radiologists using the five-point Likert scale.

Results

The CR and BV decreases with the increased of penalization factor for four hot spheres, and HYPER Iterative 2 m/b groups with penalization factor 0.07 to 0.2 had equivalent CR and better BV performance compared to OSEM 3m/b group. The liver SUV_{mean} was approximately equal in all reconstruction groups (range 5.95–5.97), and the liver CVs of HYPER Iterative 2 m/b and 3 m/b groups with the penalization factor of 0.1 to 0.2 were equivalent to OSEM 3 m/b group ($p = 0.113–0.711$ and $p = 0.079–0.287$), while the lesions SUV_{max} significantly increased 19–22% and 25% (all $p < 0.001$). The highest qualitative score was attained at the penalization factor of 0.2 for HYPER Iterative 2 m/b group (3.20 ± 0.52) and 3 m/b group (3.70 ± 0.36) which was comparable to or greater than OSEM 3m/b group (3.09 ± 0.36, $p = 0.388$ and $p < 0.001$).

Conclusions

HYPER Iterative algorithm with penalization factor of 0.2 resulted in higher lesion contrast and lower image noise in comparison with OSEM for ^{68}Ga-DOTA-NOC PET/CT, which allows lower injected activity and shorter acquisition time with preserved image quality.

Background

Positron emission tomography/computed tomography (PET/CT) imaging with ^{68}Gallium-DOTA-1-Nal3-octreotide (^{68}Ga-DOTA-NOC) is increasingly used in neuroendocrine neoplasms (NEN) [1], for its high

accuracy in the detection, staging and assessment of the primary tumor or metastasis and recurrence [2–4]. Generally, high image quality is essential to precise interpretation of PET/CT clinical studies. Bayesian penalized likelihood estimation reconstruction algorithm (BPL) has been developed and clinically implemented to improve image signal-to-noise ratio and lesion signal-to-background ratio compared to the widely used ordered subset expectation maximization (OSEM) for ^{68}Ga tracer PET [5], which is partly accountable to the full iterative convergence of the BPL algorithm without excessive noise amplification. Hence, BPL algorithm has the potential to further improve quantitation accuracy [6], shorten acquisition time [7], and reduce injected activity [8], while maintaining or even improving the image quality.

Recently, regularized expectation maximization image reconstruction, a new BPL algorithm was introduced (HYPER Iterative, United Imaging Healthcare). HYPER Iterative incorporated the pixel to pixel total variation, global noise equivalent counts, and local sensitivity profile into the penalization term, in which the only one user-adjustable parameter is the penalization factor that controls the trade-off between image noise level and resolution [9, 10]. One previous study on phantom demonstrated the potential application of HYPER Iterative for 2-deoxy-2-[^{18}F]-fluoro-D-glucose (^{18}F-FDG) PET [11]. However, a detailed analysis had not been performed on the other radiopharmaceuticals and PET/CT scanners. Therefore, we conducted a phantom and patient study to investigate the impact of different penalization factor and acquisition durations in HYPER Iterative algorithm on the image quality of ^{68}Ga-DOTA-NOC PET/CT.

Methods And Materials

Phantom data acquisition

A National Electrical Manufacturers Association (NEMA) image quality phantom was scanned on a SiPM-based digital time of fight PET/CT scanner (uMI780, United Imaging Healthcare). Four smallest spheres of the phantom (diameter =10, 13, 17 and 22 mm) were filled with 13.2 kBq/mL of ^{68}Ga solution, and the concentration of the hot sphere was 4 times that of the background, then the list-mode data were acquired after 120 min of waiting time.

The phantom data were acquired in a list mode with matrix192×192 and an axial field of view 30 mm. The images were reconstructed using recommended standard OSEM protocol by the manufacturer (Two iterations, 20 subsets, 3 mm Gaussian filter, time of fight, point spread function model, scatter, CT attenuation and other necessary corrections) and HYPER Iterative (Seven penalization factors: 0.03, 0.07, 0.1, 0.2, 0.3, 0.4, 0.5) with 31 and 46 seconds duration of list-mode data whose counts were comparable to the clinical acquisition protocols using 2 and 3 minutes per bed position (m/b). Thus, PET images were reconstructed in a total of 16 groups which named as O2 and O3 for OSEM with 2 and 3 m/b simulated data; HR2.03, HR2.07, HR2.1, HR2.2, HR2.3, HR2.4, HR2.5, HR3.03, HR3.07, HR3.1, HR3.2, HR3.3, HR3.4, and HR3.5 for HYPER Iterative with 2 and 3 m/b and penalization factors range from 0.03 to 0.5, respectively.

Phantom data evaluation

The data were measured by percent contrast recovery (CR) and background variability (BV) for each sphere using NEMA NU2-2012 image quality analysis tool (United Imaging Healthcare), shown in equation 1-2. The radioactivity counts of each hot sphere were measured by placing a region of interest (ROI) on the sphere matched to the sphere diameter, and the standard deviation (SD) of phantom background counts was estimated by placing ROIs in the peripheral area of the phantom background at the center slice of the spheres. Meanwhile, the normalized activity of each hot sphere was calculated by the mean activity concentrations of all reconstruction groups over that of O3, which revealed the relative change resulted from the different reconstructions using O3 as the reference.

$$CR_{H,j} = (C_{H,j}/C_{B,j} - 1)/(a_H/a_B - 1) \times 100\% \quad (1)$$

$$BV_j = SD_j/C_{B,j} \times 100\% \quad (2)$$

Where $CR_{H,j}$ is the percent CR of the sphere *j*, $C_{H,j}$ and $C_{B,j}$ are the average counts within a ROI on each sphere *j* and corresponding background ROIs. a_H and a_B are the activity concentration in the sphere and the background of the phantom, BV_j is the percent *BV* measured by background ROIs from sphere *j*, SD_j is the standard deviation of the background ROI counts for sphere *j*.

Patients

Twenty-five patients (Ten men, fifteen women) admitted to Nanjing First Hospital between March 16 and June 16 of 2021 undergoing ^{68}Ga-DOTA-NOC PET/CT imaging, were consecutively enrolled in this retrospective study. The inclusion criteria were as follows: the NEN was identified by pathology; ^{68}Ga-DOTA-NOC avid lesions were found on PET images; the informed consent was wavered. The patient with visible liver metastases or unavailable raw data was excluded. The clinical study was approved by the ethics committee of Nanjing first hospital, Nanjing medical university (KY20171208-02) and performed in accordance with the principles of the declaration of Helsinki and national regulations. The mean age of the patients was 54.6 ± 12.2 years. The patient weight was 61.3 ± 9.7 kg, and the height was 1.63 ± 0.06 m. Seven patients were diagnosed with adrenal pheochromocytoma, three with paraganglioma, six with pancreatic NEN, four with lung NEN, three with rectal NEN, and two with retroperitoneal NEN. The details of patient characteristics were listed in Table 1.

Clinical image acquisition

The clinical acquisition protocol of ^{68}Ga-DOTA-NOC PET/CT was with the same as those described in the phantom study. The patients received 1.01-2.43 MBq/kg of ^{68}Ga-DOTA-NOC and rested for approximately 66 minutes after administration (Table 1). PET/CT imaging was conducted from the skull base to upper thigh in 3D list mode with 3 m/b of acquisition time which was also reconstructed into 2 m/b. The PET

image reconstruction setting and naming rules of 16 reconstruction groups were in accord with the phantom study.

Quantitative evaluation of clinical images

The PET image quality was quantitatively assessed using image noise level which was defined as percent coefficient of variation (CV) in the liver. A 3 cm diameter sphere volume of interest (VOI) was firstly drawn on O3 in the place of uniform liver tissue to avoid hepatic porta and large portal vessels, then copied and pasted to the other reconstruction groups, thus the mean and standard deviation of standard uptake value (SUV_{mean}) and SUV_{sd} were automatically measured. The percent CV was calculated by SUV_{sd} over SUV_{mean}. The normalized CV was defined by the ratio of CV for all groups to that for O3. Moreover, the lesion was delineated with a semi-automatic 3D segmentation tool by a nuclear radiologist, thus the maximum of standard uptake value (SUV_{max}) and the volume of the lesion were measured, meanwhile SUV_{max} normalization was also performed in the same calculation as CV. The equivalent diameter (*D*) of the lesion was calculated as diameter of a sphere that had a same volume of the lesion.

Qualitative assessment of clinical images

The PET images were independently evaluated by two nuclear radiologists with 10 years' experience in a dedicated workstation (uWS-MI R004, United Imaging Healthcare). All images were anonymized and ranked without knowing the reconstruction setting, and the reading numbers were randomly assigned so as to reduce the bias. PET datasets were rated using five-point Likert scale (1= poor image quality with excessive noise or unnatural texture, and insufficient lesion depiction. 2= unacceptable image quality with suboptimal noise, or poor lesion contrast and delineation leading to low diagnostic confidence. 3= acceptable image quality with appropriate noise, sufficient lesion delineation and natural image texture to make a diagnosis. 4= good image quality with optimal noise and satisfactory lesion delineation resulting in full diagnostic confidence. 5= excellent image quality with almost free of noise, perfect contrast for the lesion to background and sharp border for the lesion or organs delineation).

Statistical analysis

GraphPad Prism 8 and Microsoft Excel 2016 were used for all statistical analysis. The data were presented as mean ± SD. Since the precise measurement of true SUV was difficultly known in the patient study, the SUV of O3 was stetted as the reference for the comparison between different reconstruction groups. Paired t-test was applied in comparing the difference of lesion SUV_{max} between O3 and the other reconstruction groups which fitted normal distribution according to D'Agostino & Pearson normality test. Wilcoxon matched-pairs signed rank test was used to examined the difference of liver CV and visual image quality score between O3 and the other reconstruction groups. The p-value was adjusted with Benjamin & Hochberg correction to control the false discovery rate due to multiple comparisons. The

inter-rater agreement on the visual image quality scores was measured by Cohen's Kappa test. In all analysis, $p < 0.05$ was considered to indicate statistical significance.

Results

Phantom study

The CRs of four hot spheres decreased with the increase of the penalization factors except HR2.3, and a slight decline of HR3.03 to HR3.5 was observed in three large hot spheres with the diameter of 22 mm (85.4-83.8), 17 mm (77.0-74.4) and 13 mm (78.3-75.2) (Figure 1a). The CRs of HR3.07 to HR3.1were higher than those of O3 for four spheres. The CRs was the highest in the diameter of 22 mm hot sphere, second in 17 mm, third in 13 mm, lowest in 10 mm for HR2.03 to HR2.5, but the CRs in the diameter of 13 mm hot sphere were slightly higher than those attained in the diameter of 17 mm hot sphere for HR3.03 to HR3.5 (Figure 1a). Moreover, the mean of normalized activity was higher than 1.0 for HR2.03 to HR2.07(1.00-1.01), and HR3.03 to HR3.4 (1.01-1.05), the mean of normalized activity was very close to 1.0 for HR2.1 (0.996) and HR3.5 (0.998), and the mean of normalized activity of HR2.2 to HR2.5 (0.92-0.97) was less than 1.0 (Figure 2a).

The BVs decreased along with the increase of the penalization factors for each hot sphere. Moreover, the BVs of O2 were higher than O3 and HYPER iterative 2 m/b and 3m/b groups at the same diameters. The BVs were lowest for 22-mm-diameter sphere, followed by 17 mm and 13 mm diameter spheres, and highest for 10-mm-diameter sphere with the same reconstruction method. The BVs of HR2.03 were higher than those of O3 at the same diameter, and the BVs of HR2.07 and HR2.1 were comparable to O3, because the difference was limited to a small range (-1.0 % -0.7 %). Furthermore, the BVs of other HYPER iterative groups (HR2.2 to HR2.5 and HR3.03 to HR3.5) had better performance than O3 (Figure 1b).

Quantitative analysis of clinical study

The average liver SUV_{mean} was approximately equal in all reconstruction groups, it was 5.95 for O2, 5.96 for O3 and HR2.03 to HR2.5, and 5.97 for HR3.03 to HR3.5, respectively (Table 2). The CVs of all reconstruction groups had less than 15 %. In detail, the highest CV of liver was 14.36 ± 3.38 % and 12.88 ± 3.26 % for O2 and O3, respectively (Table 2). The CV declined from 14.00 ± 3.00 % to 10.59 ± 3.23 % for HR2.03 to HR2.5, and from 13.52 ± 2.99 % to 10.96 ± 3.11 % for HR3.03 to HR3.5 (Table 2). The HR2.1, HR2.2, HR3.1, and HR3.2 groups were considered noise equivalent groups to O3, because their CVs didn't make a significant difference (p=0.113, 0.711, 0.079, and 0.287), and the image noise of HR2.03 and HR3.03 was equivalent to O2 (p=0.525 and 0.055). The CVs of HR2.03, HR2.07, HR3.03, and HR3.07 group were significantly higher than that of O3 (all p<0.01), whereas the CVs of HR2.3 to HR2.5 and HR3.3 to HR3.5 were significantly lower than O3 (all p<0.01). Moreover, the mean of normalized CV was range from 0.83 to 1.12 for HR2.03-HR2.5 and 0.85 to 1.06 for HR3.03-HR3.5 (Table 2). The standard deviation of normalized CV was lowest for HR3.03-HR3.1 (all 0.07), and increased with the increased of penalization factor.

The lesion SUV_{max} decreased with the increase of the penalization factors except for HR2.1 (Table 2). The lesion SUV_{max} of all HYPER Iterative 2m/b and 3 m/b groups was significantly higher than that of O3 (all $p<0.001$), and the lesion SUV_{max} of O2 (10.29 ± 6.14) was comparable to that of O3 (10.28 ± 6.01). The mean of normalized SUV_{max} for HYPER Iterative groups with 3 m/b was higher than those with 2 m/b when the penalization factor was the same. In detail, the mean of lesions SUV_{max} increased 22 % - 18 % for HR2.03 to HR2.5, and 25 % -23 % for HR3.03 to HR3.5 compared to O3, respectively (Table 2 and Figure 2b).

The lesions were first divided into small (D<10 mm, n=13, range 7.7-9.9 mm), medium (10 ≤

D<20 mm, n=57, range 10.1-19.7 mm), and large categories (D≥20 mm, n=13, range 20.3-27.3 mm) according to their equivalent diameters. The mean of normalized lesion SUV_{max} slightly decreased with the increased penalization factor for each category, and the mean of normalized SUV_{max} for small lesions was higher than those for medium and large lesions in all HYPER iterative 2 m/b and 3 m/b groups except for HR2.4 and HR2.5 at the same penalization factor and acquisition time (Figure 3a). Minor change of average normalized SUV_{max} was found for large lesions in all HYPER iterative groups, and the minor change was also found for the medium lesions. The mean of normalized SUV_{max} was higher than 1.0 for large lesions (range 1.06-1.11) and 1.2 for medium lesions (range 1.20-1.23) in all HYPER iterative groups, respectively. Meanwhile, the mean of normalized SUV_{max} for small lesionswas range from 1.19 to 1.25 in HR2.03-HR2.5 and increased to 1.45-1.47 in HR3.03-HR3.5.

The effect of the injected activity (IA) on the lesion SUV_{max} of different reconstruction is demonstrated in Figure 3b. The lesions were classified into low (IA< 1.60 MBq/kg, n=35, range 1.01-1.59 MBq/kg) and large injected activity (IA≥1.60 MBq/kg, n=45, range 1.61-2.43 MBq/kg) according to our previous research and PET detection performance [12]. The mean of normalized SUV_{max} for high injected activity groups was slightly higher than that for low injected activity in all HYPER iterative groups except for HR2.3-H2.5 (Figure 3b). Detailly, the mean of normalized lesion SUV_{max} for all HYPER iterative groups floated around 1.2, the range was 1.19-1.23 for low activity and 1.18-1.27 for high activity. The mean of normalized SUV_{max} of HR3.03 to HR3.5 was comparable and a little higher than that of HR2.03 to HR2.5 for low and large injected activity, respectively.

To investigate the effect of patient weight on the lesion SUV_{max}, the patients were further sorted into two categories by body mass index (BMI): under-and-normal weight group (BMI <24 kg/m^2, n=47, range 18.36-23.72 kg/m^2) and overweight group (BMI≥24 kg/m^2, n=33, range 24.22-28.12 kg/m^2). The mean of normalized lesion SUV_{max} for under-and-normal weight group was higher than that for overweight group in the HYPER iterative 2m/b groups at the same penalization factor, while the trend was contrary with 3m/b acquisition. Additionally, the mean of normalized lesion SUV_{max} had small changes between two BMI-categories in all HYPER iterative groups with the same penalization factor and acquisition time, but obvious increase was found in the HYPER iterative groups with 3 m/b acquisition compared to 2 m/b

(Figure 3c). The mean of normalized lesion SUV_{max} was higher than 1.2 (range 1.20-1.23) and 1.15 (range 1.15-1.27) for under-and-normal weight group and overweight group with HYPER Iterative, respectively.

A total of 80 ^{68}Ga-DOTANOC avid lesions were identified: Eight lesions in the lung, 38 in the bone, two in the thyroid, 27 in the lymph node, four in the soft issue, and one in the pancreas. The mean of normalized SUV_{max} was weakly decreased with the increased penalization factor for lung, lymph node and bone metastases. Moreover, the mean of normalized SUV_{max} for HYPER Iterative groups with 3 m/b acquisition was higher than that with 2 m/b when the lesion location and the penalization factor were the same. Of note, the mean of normalized lesion SUV_{max} was highest in bone, second in lymph node, lowest in lung at the same penalization factor. Furthermore, the mean of normalized lesion SUV_{max} was higher than 1.0 (range 1.07-1.18) for lung, 1.1 (range 1.11-1.21) for lymph node, and 1.2 (range 1.26-1.30) for bone with HYPER Iterative, respectively. (Figure 3d).

Qualitative image quality of clinical study

The mean of image quality score was first increased then declined with the increased of the penalization factors (Figure 4). The highest image quality score was assigned to HR2.2 (3.20 ± 0.52) and HR3.1 (3.70 ± 0.36) for 2 m/b and 3 m/b acquisition groups. The lowest score was acquired at HR2.4 (2.44 ± 0.45) and HR2.5 (2.16 ± 0.35) due to poor contrast for small lesions (Figure 7 and Figure 9), and the secondary score was given to O2 (2.81± 0.35) because of suboptimal image noise (Figure 5, Figure 6, and Figure 8). The average scores of HR3.07 to HR3.3 were significantly high than that of O3 (all $p<0.05$), and the image quality scores of HR2.07 to HR2.3 did not differ from O3 (all $p>0.062$). The inter-rater agreement was substantial ($k=0.71$).

Discussion

We investigated the effect of HYPER Iterative algorithm on the image quality of ^{68}Ga-DOTA-NOC PET/CT and focus on determining the optimal penalization factor using the phantom and patient data. HYPER Iterative 2 m/b groups with a penalization factor between 0.07 and 0.2 could offer 19–22% lesion SUV_{max} growth and 0–10% lower noise compared to OSEM 3m/b group while saving one-third acquisition time. Our qualitative and quantitative results suggested that a penalization factor of 0.2 could provide the optimal image quality for ^{68}Ga-DOTA-NOC PET/CT with lower image noise and higher lesion contrast for different size lesion, patient weight, injected activity, and tumor location.

Inappropriate selection of penalization factor may overestimate or under-estimate the noise, and results in over-smoothed or under-convergent image [13]. The choice of the optimal penalization factor was challenging and usually affected by the radiopharmaceutical, the acquisition setting, radiologists' preference, BPL algorithms' tiny difference, and measures of image quality. Therefore, the optimal penalization factor is often given as a reference range. The phantom and clinical ^{18}F-FDG studies indicated that BPL with the penalization factor between 500 and 600 could provide better quantitation

accuracy and image quality compared to OSEM [14]. For ^{68}Ga tracer, one preliminary study suggested BPL algorithm with a penalization factor between 350 and 450 could be used in clinical practice for all studied radiopharmaceuticals [15], while a ^{68}Gallium-DOTA0-1NaI3-octreotide(^{68}Ga-DOTA-TOC) PET study recommended that a factor equal to 400 or higher than 400 could be optimal [16]. However, another ^{68}Gallium-DOTA0-Tyr3-octreotate (^{68}Ga-DOTA-TATE) PET/CT study concluded that BPL algorithm with the penalization factor within 1100 to 1400 with 1.5 m/b resulted in better image quality than OSEM, while choosing from 1300 to 1600 for 1 m/b also had better image quality [17]. In line with those studies, our study suggested a penalization factor between 0.03 and 0.5 for HYPER Iterative reconstruction that provided higher lesion contrast compare to OSME, while lower image noise was acquired between 0.1 and 0.5. Moreover, both HYPER Iterative 2 m/b and 3 m/b acquisitions with a penalization factor between 0.1 and 0.2 could attain equivalent image noise to OSME 3 m/b acquisition. Therefore, the recommended penalization factors should be always be accompanied by the radiopharmaceutical, the acquisition settings and criteria for the optimal image quality, for they may change the choice of the penalization factor.

Our data inferred the SUV_{max} of the large lesions (> 20 mm) increased more than 6% in all HYPER Iterative 2 m/b and 3 m/b groups compared to OSEM 3 m/b group, and a 20% increase was found for medium lesions ($10 \leq D < 20$ mm), meanwhile the SUV_{max} of the small lesions (< 10) increased more than 19% for all HYPER Iterative 2 m/b groups, and the increase reached up to 45% for 3 m/b groups. Those results were in accordance with the findings of a previous study using ^{68}Gallium-labeled tracer targeting the prostate-specific membrane antigen (^{68}Ga-PSMA) PET/CT in which the contrast of the large lesions ((> 20 mm) increased 10% in BPL algorithm with a penalization factor of 0.14 compared to OSEM, while the increase was 20% for small lesions (< 20 mm) [18]. Additionally, another study using ^{18}F-FDG PET/CT in which the conspicuity and SUV_{max} of lung lesion < 10 mm in diameter on image reconstructed by BPL algorithm were significantly higher than those with OSEM [19], while those significant increases were not found on the lesions > 10 mm in diameter between BPL and OSEM. Therefore, our results and the others supported BPL-based algorithm could improve the small lesion contrast and conspicuity regardless of the difference criteria for small lesions.

According to the recommended activity of current procedure guidelines for ^{68}Ga-DOTA-conjuated peptides ranges from 100 to 300 MBq depending on the PET tomography characteristics, and to obtain a good image quality is at least 100 MBq [20]. Our data showed regardless of injected activity per kilogram, HYPER Iterative had higher lesions SUV_{max} compared to OSEM, but the penalization factor had limited influence on the gain of lesion SUV_{max} between the HYPER Iterative groups with the same acquisition time, and lesion SUV_{max} was a bit increase with extending acquisition time from 2 m/b to 3 m/b, these results were in accordance with a previous study which evaluate the influence of different penalization factor for different activity time products in whole-body ^{18}F-FDG PET/CT [14]. Of note, the average injected activity of our study was less than 100 MBq, which may have potentials to reduce patient dose and acquisition time.

Increasing patient weight may cause an increasing noise and consequent affect the quality of PET images [21]. A previous study of ^{18}F-FDG showed BPL algorithm provided a more consistent liver signal-to noise ratio than dose OSEM with increasing patient BMI [22]. Our study demonstrated that with the increasing of penalization factor, the gains gap of lesions SUV_{max} were minor and relatively stable in two BMI-groups for 2 m/b and 3 m/b acquisition. Moreover, the gains of lesions SUV_{max} were nearly equivalent for normal-and-underweight patients with the increasing of penalization factor, but the relative difference between 2 m/b and 3m/b groups was lager for overweight patients with the same penalization factor, which means that higher weight patients benefit much more from the HYPER Iterative reconstruction with longer acquisition.

No previous studies have been performed on the impact of BPL algorithm on the lesions location of PET imaging. Our study found that the gain of lesion SUV_{max} was highest for bone, second for lymph node, lowest for lung with the same penalization factor, but the gains of SUV_{max} were higher for lung and lymph nodes between 2 m/b and 3 m/b acquisition, which may result from tumor uptake and patient characteristics.

Shorter acquisition time is important to patient comfort and throughput in any busy clinical. Previous studies have proved that BPL algorithm had the capability on shortening acquisition time in ^{18}F-FDG and ^{68}Ga tracer PET/CT imaging [23–25]. Our results indicated that HYPER Iterative algorithm could enable one third reduction of time duration of ^{68}Ga-DOTA-NOC PET with equivalent or improved image quality compared to 3 m/b OSEM. However, more studies were needed to explore the potential of BPL algorithm on improving lesion conspicuity of malignant tumors or maintaining the image quality for delayed PET imaging.

The results of qualitative image quality ranked by nuclear radiologists depends on several factors: the personal experience, clinical task, image noise and contrast. In our study, the highest average quality score was given to the penalization factor of 0.2 for both 2 m/b and 3 m/b acquisition. The selection penalization factor was equal to or higher than the noise equivalent groups (HR2.1 to HR2.2 and HR3.1 to HR3.2). Although the coefficients of variation of all the HYPER Iterative groups were less than the recommended maximal tolerance (15%) in our clinical practice. The ranker often preferred the image with lower background noise level while maintaining higher tumor to background contrast, because it could promote the diagnostic confidence for detecting all malignancies, especially for the small and low contrast lesions. We also noted that the image noise level was less than 13% when the image quality score was highest at a penalization factor of 0.2. In addition, further increasing penalization factor might produce smoother images, but result in less contrast enhancement, pointing out that this noise level should be considered as the target noise setting for acquiring high quality images in ^{68}Ga-DOTA-NOC PET/CT practice. This phenomenon was consistent with previous studies using BPL algorithm on ^{68}Ga tracer PET with high penalization factor [12, 18].

In clinical practice, the penalization factor should be fixed to maintain the consistency of SUV. In a previous study of ^{68}Ga-DOAT-TATE PET, the optimal penalization factor was determined from the equivalent noise group which had increased tumor SUV_{max} and improved signal-to-background ratio [17], while it also depended on lesion detection rate and a high patient throughput in oncologic whole-body ^{18}F-FDG examinations [14]. Since the radiologists remain the intention to diagnosis as center task, it must be appropriate to consider the raters' preference on the choosing of optimal noise penalization factor. Therefore, our study recommended a penalization factor of 0.2 for 2 m/b and 3 m/b acquisition as the optimal choice through comprehensive analysis, which provided a fine balance of visual assessment and quantitative evaluation.

Our study has several limitations. First, only 25 patients were included in this work due to the time-consuming task of the image reconstruction with different penalization factor. A larger number of suspected or untreated NENs patients should be involved in future studies. Second, the relationship between SUV measurement under HYPER Iterative reconstruction and pathological results need to be investigated, which could benefit early differential diagnosis of NENs. Furthermore, the ability of noise smoothing by HYPER Iterative algorithm could be applied to dynamic PET imaging or late-phase imaging for lesion detection.

Conclusions

HYPER Iterative reconstruction algorithm with a penalization of 0.2 can improve lesion contrast as well as lower image noise of ^{68}Ga-DOTA-NOC PET/CT compared to OSME, which hence enable shorten the acquisition time and reduce the injected activity with maintaining the image quality.

Abbreviations

^{68}Ga-DOTA-NOC: ^{68}Gallium-DOTA0-1Nal3-octreotide; PET: PET/CT: positron emission tomography/computed tomography; NEN: neuroendocrine neoplasms; BPL: Bayesian penalized likelihood; OSEM: ordered subset expectation maximization; ^{18}F-FDG: 2-deoxy-2-[^{18}F]-fluoro-D-glucose; NEMA: National Electrical Manufacturers Association; CR: contrast recovery; BV: background variability; ROI: region of interest; VOI: volume of interest; SD: standard deviation; SUV: standard uptake value; HR: HYPER iterative; D: equivalent diameter; CV: coefficient of variation; ^{68}Ga-PSAM: ^{68}Gallium-labeled tracer targeting the prostate-specific membrane antigen; ^{68}Ga-DOTA-TOC: ^{68}Gallium-DOTA0-1Nal3-octreotide; ^{68}Ga-DOTA-TATE: ^{68}Gallium-DOTA0-Tyr3-octreotate

Declarations

Ethical approval and consent to participate

The study was approved by the institute ethical review board of Nanjing Medical University, Nanjing First Hospital (KY20171208-02) and performed in accordance with the principles of declaration of Helsinki

and national regulations. Informed consent was obtained from all individual participants or legal guardians included in the study.

Consent for publication

Patients signed informed consent regarding publishing their data and photograhs.

Availability of data and materials

The datasets used and analyzed during the current study are available from the corresponding author on reasonable request.

Competing interests

The authors declare that there is no conflict of interests regarding the publication of this paper.

Funding

This research was supported by grants from National Natural Science Foundation of China (11805104), Jiangsu Provincial Frontier Grant (BE2017612), and Nanjing Municipal Health Science and Technology Development Fund (YKK20104).

Authors' contributions

LX and CC write the manuscript and performed the data analysis. RY and RL carried out data acquisition. RL carried out the image interpretation. FW and QM carried out the conception and design. All authors read and approved the final manuscript.

Acknowledgments

We thank all members of the research group.

References

1. Purandare NC, Puranik A, Shah S, et al. Differentiating dural metastases from meningioma: role. of 68Ga DOTA-NOC PET/CT. Nucl Med Commun. 2020;41(4):356–62.
2. Calabrò D, Allegri V, Fanti S, et al. ^{68}Ga-DOTANOC and ^{18}F-DOPA PET/CT: a site-specific approach to the imaging of parangliomas of the head and neck and of the abdomen. Eur J Nucl Med Mol Imaging. 2019;46(6):1393.
3. Yadav D, Ballal S, Yadav MP, et al. Evaluation of [^{68}Ga]Ga-DATA-TOC. for imaging of neuroendocrine tumours: comparison with [^{68}Ga]Ga-DOTA-NOC PET/CT. Eur J Nucl Med Mol Imaging. 2020;47(4):860–9.

4. Lamarca A, Pritchard DM, Westwood T, et al. 68Gallium DOTANOC-PET Imaging in Lung Carcinoids: Impact on Patients' Management. Neuroendocrinology. 2018;106(2):128–38.
5. Rijnsdorp S, Roef MJ, Arends AJ. Impact of the Noise Penalty Factor on Quantification in. Bayesian Penalized Likelihood (Q.Clear) Reconstructions of ^{68}Ga-PSMA PET/CT Scans. Diagnostics (Basel). 2021;11(5):847.
6. Wu Z, Guo B, Huang B, et al. Phantom and clinical assessment of small pulmonary nodules using Q.Clear reconstruction on a silicon-photomultiplier-based time-of-flight PET/CT system. Sci Rep. 2021;11(1):10328.
7. Svirydenka H, Muehlematter UJ, Nagel HW, et al. 68Ga-PSMA-11 dose reduction for dedicated pelvic imaging with simultaneous PET/MR using TOF BSREM reconstructions. Eur Radiol. 2020;30(6):3188–97.
8. Rogasch JM, Suleiman S, Hofheinz F, et al. Reconstructed spatial resolution and contrast recovery with Bayesian penalized likelihood reconstruction (Q.Clear) for FDG-PET compared to time-of-flight (TOF) with point spread function (PSF). EJNMMI Phys. 2020;7(1):2.
9. Baratto L, Duan H, Ferri V, Khalighi M, Iagaru A. The Effect of Various β Values on Image Quality and Semiquantitative Measurements in 68Ga-RM2 and 68Ga-PSMA-11 PET/MRI Images Reconstructed With a Block Sequential Regularized Expectation Maximization Algorithm. Clin Nucl Med. 2020;45(7):506–13.
10. Xie Z, Baikejiang R, Li T, et al. Generative adversarial network based regularized image reconstruction for PET. Phys Med Biol. 2020;65(12):125016.
11. Tatsumi M, Soeda F, Kamiya T, et al. Effects of New Bayesian Penalized Likelihood Reconstruction Algorithm on Visualization and Quantification of Upper Abdominal Malignant Tumors in Clinical FDG PET/CT Examinations. Front Oncol. 2021;11:707023.
12. Xu L, Zhou LL, Zhao ZY, et al. Acquisition Protocols to Optimize ^{68}Ga-DOTA-NOC Position. Emission Tomography/Computer Tomography Image Quality Based on Patient Body Mass Index and Injected Dose[J]. J Med Imaging Health Inform. 2020;10(2):508–14.
13. Ter Voert EEGW, Muehlematter UJ, Delso G, et al. Quantitative performance and optimal. regularization parameter in block sequential regularized expectation maximization reconstructions in clinical ^{68}Ga-PSMA PET/MR. EJNMMI Res. 2018;8(1):70.
14. Trägårdh E, Minarik D, Almquist H, et al. Impact of acquisition time and penalizing factor in. a block-sequential regularized expectation maximization reconstruction algorithm on a Si-photomultiplier-based PET-CT system for ^{18}F-FDG. EJNMMI Res. 2019;9(1):64.
15. Lantos J, Mittra ES, Levin CS, et al. Standard OSEM vs. regularized PET image reconstruction: qualitative and quantitative comparison using phantom data and various clinical radiopharmaceuticals. Am J Nucl Med Mol Imaging. 2018;8(2):110–8.
16. Lindström E, Lindsjö L, Sundin A, et al. Evaluation of block-sequential regularized expectation maximization reconstruction of 68Ga-DOTATOC, 18F-fluoride, and 11C-acetate whole-body examinations acquired on a digital time-of-flight PET/CT scanner. EJNMMI Phys. 2020;7:40.

17. Chicheportiche A, Goshen E, Godefroy J, et al. Can a penalized-likelihood estimation algorithm be used to reduce the injected dose or the acquisition time in ^{68}Ga-DOTATATE PET/CT studies? EJNMMI Phys. 2021;8(1):13.
18. Yang FJ, Ai SY, Wu R, et al. Impact of total variation regularized expectation maximization reconstruction on the image quality of ^{68}Ga-PSMA PET: a phantom and patient study. Br J Radiol. 2021;94(1120):20201356.
19. Kurita Y, Ichikawa Y, Nakanishi T, et al. The value of Bayesian penalized likelihood. reconstruction for improving lesion conspicuity of malignant lung tumors on ^{18}F-FDG PET/CT: comparison with ordered subset expectation maximization reconstruction incorporating time-of-flight model and point spread function correction. Ann Nucl Med. 2020;34(4):272–9.
20. Bozkurt MF, Virgolini I, Balogova S, et al. Guideline for PET/CT imaging of. neuroendocrine. neoplasms with 68Ga-DOTA-conjugated somatostatin receptor targeting peptides and 18F-DOPA. Eur J Nucl Med Mol Imaging. 2017;44(9):1588–601.
21. Taniguchi T, Akamatsu G, Kasahara Y, et al. Improvement in PET/CT image quality in. overweight patients with PSF and TOF. Ann Nucl Med. 2015;29(1):71–7.
22. Chilcott AK, Bradley KM, McGowan DR. Effect of a Bayesian Penalized Likelihood PET. Reconstruction Compared with Ordered Subset Expectation Maximization on Clinical Image Quality Over a Wide Range of Patient Weights. AJR Am J Roentgenol. 2018;210(1):153–7.
23. Lindström E, Sundin A, Trampal C, et al. Evaluation of Penalized-Likelihood Estimation Reconstruction on a Digital Time-of-Flight PET/CT Scanner for ^{18}F-FDG Whole-Body Examinations. J Nucl Med. 2018;59(7):1152–8.
24. Bjöersdorff M, Oddstig J, Karindotter-Borgendahl N, et al. Impact of penalizing factor in a block-sequential regularized expectation maximization reconstruction algorithm for ^{18}F-fluorocholine PET-CT regarding image quality and interpretation. EJNMMI Phys. 2019;6(1):5.
25. Lindström E, Velikyan I, Regula N, et al. Regularized reconstruction of digital time-of-flight ^{68}Ga-PSMA-11 PET/CT for the detection of recurrent disease in prostate cancer patients. Theranostics. 2019;9(12):3476–84.

Tables

Table 1
Patient characteristics

Characteristics	Values
Sex	Male 10; Female 15
Age	54.6 ± 12.2 [35, 79] years
Height	1.63 ± 0.06 [1.55, 1.78] m
Weight	61.3 ± 9.7 [47.1, 80.0] kg
Body Mass index	22.9 ± 2.6 [18.3, 28.1] kg/m^2
Uptake Time	66.3 ± 15.3 [47, 97] minutes
Injected Activity	97.2 ± 19.7 [55.7, 129.4] MBq
Injected Activity Per kilogram	1.6 ± 0.3 [1.0, 2.4] MBq/kg
Primary tumor	Pheochromocytoma (n = 7), Paraganglioma (n = 3), Pancreatic NET (n = 6), Lung NET (n = 4), Rectal NET (n = 3), Retroperitoneal NET (n = 2).

Table 2. SUV_{mean}, CV of liver, and lesion SUV_{max}, Normalized lesion SUV_{max} of the clinical study

Group	SUV_{mean} of Liver	CV (%) of liver	Normalized CV	SUV_{max} of lesions	Normalized of SUV_{max}
O2	5.95 ± 1.01	14.36 ± 3.38	1.12 ± 0.08	10.29 ± 6.14	1.00 ± 0.08
R2.03	5.96 ± 1.01	14.00 ± 3.00	1.10 ± 0.11	12.37 ± 6.95	1.22 ± 0.20
R2.07	5.96 ± 1.01	13.60 ± 2.98	1.07 ± 0.11	12.35 ± 6.96	1.22 ± 0.20
R2.1	5.96 ± 1.01	13.33 ± 3.03	1.05 ± 0.12	12.36 ± 6.95	1.22 ± 0.20
R2.2	5.96 ± 1.01	12.55 ± 3.08	0.98 ± 0.12	12.28 ± 7.00	1.19 ± 0.24
R2.3	5.96 ± 1.01	11.74 ± 3.11	0.92 ± 0.13	12.23 ± 7.03	1.20 ± 0.28
R2.4	5.96 ± 1.01	11.13 ± 3.16	0.87 ± 0.14	12.16 ± 7.05	1.19 ± 0.23
R2.5	5.96 ± 1.01	10.59 ± 3.23	0.83 ± 0.14	12.09 ± 7.10	1.18 ± 0.23
O3	5.96 ± 1.00	12.88 ± 3.26	1.00 ± 0.00	10.28 ± 6.01	1.00 ± 0.00
R3.03	5.97 ± 1.00	13.52 ± 2.99	1.06 ± 0.07	12.58 ± 6.71	1.25 ± 0.17
R3.07	5.97 ± 1.00	13.23 ± 2.98	1.04 ± 0.07	12.57 ± 6.71	1.25 ± 0.17
R3.1	5.97 ± 1.00	13.05 ± 3.00	1.02 ± 0.07	12.57 ± 6.71	1.25 ± 0.17
R3.2	5.97 ± 1.00	12.45 ± 2.98	0.97 ± 0.08	12.54 ± 6.72	1.25 ± 0.17
R3.3	5.97 ± 1.00	11.89 ± 3.01	0.93 ± 0.09	12.51 ± 6.73	1.24 ± 0.17
R3.4	5.97 ± 1.00	11.42 ± 3.05	0.89 ± 0.10	12.48 ± 6.74	1.24 ± 0.17
R3.5	5.97 ± 1.00	10.96 ± 3.11	0.85 ± 0.11	12.46 ± 6.76	1.23 ± 0.17

Figures

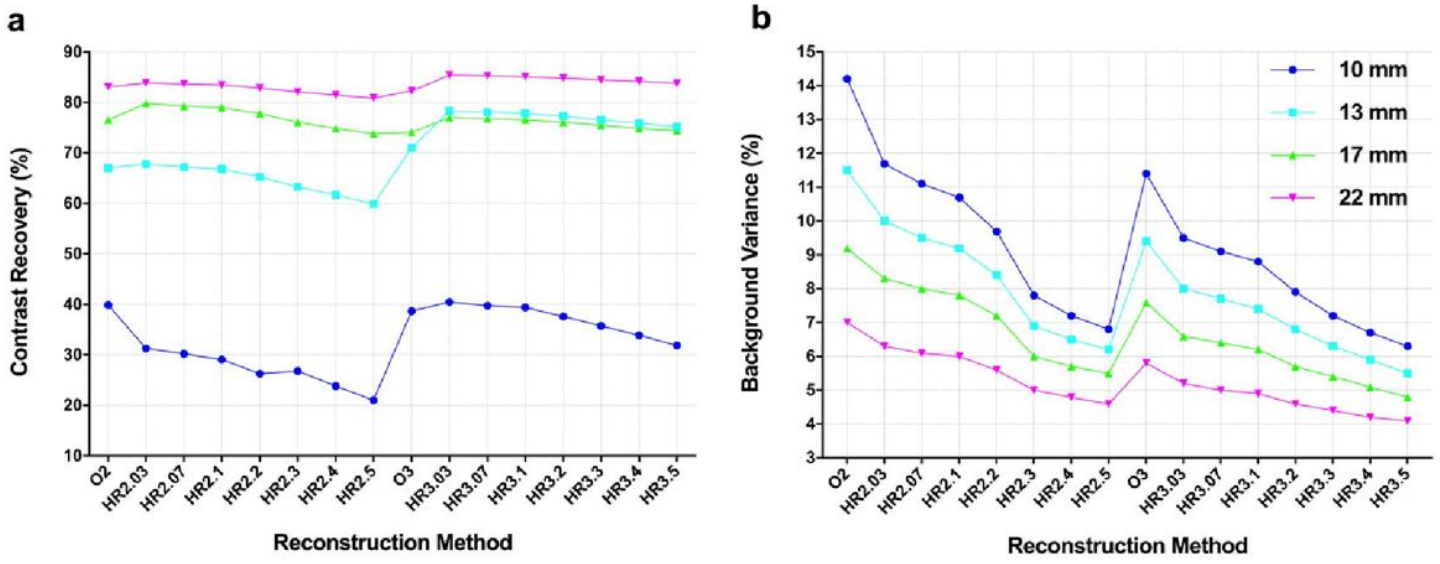

Figure 1

The plot of contrast recovery (a) and background variance (b) with different PET reconstruction methods for 4 hot spheres in the phantom.

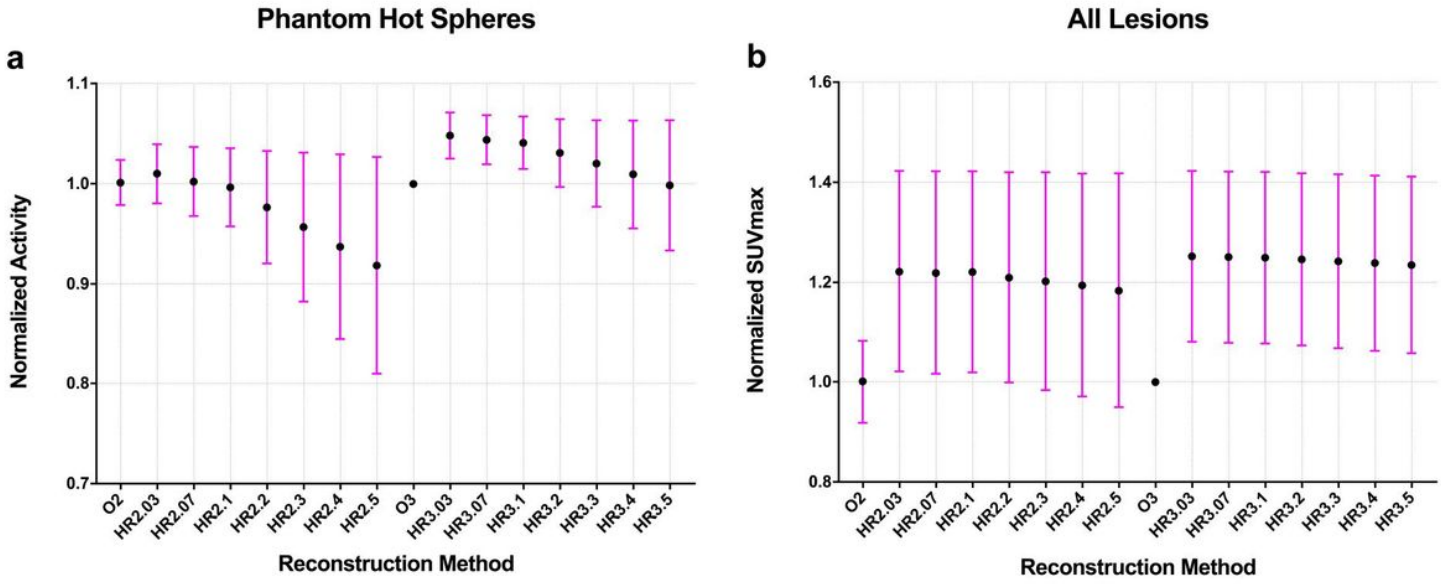

Figure 2

The relationship between normalized SUV_{max} and reconstruction methods. (a) The mean and SD of normalized activity change for the 4 hot spheres in the phantom study. (b) The mean and SD of normalized SUV_{max} for all lesions.

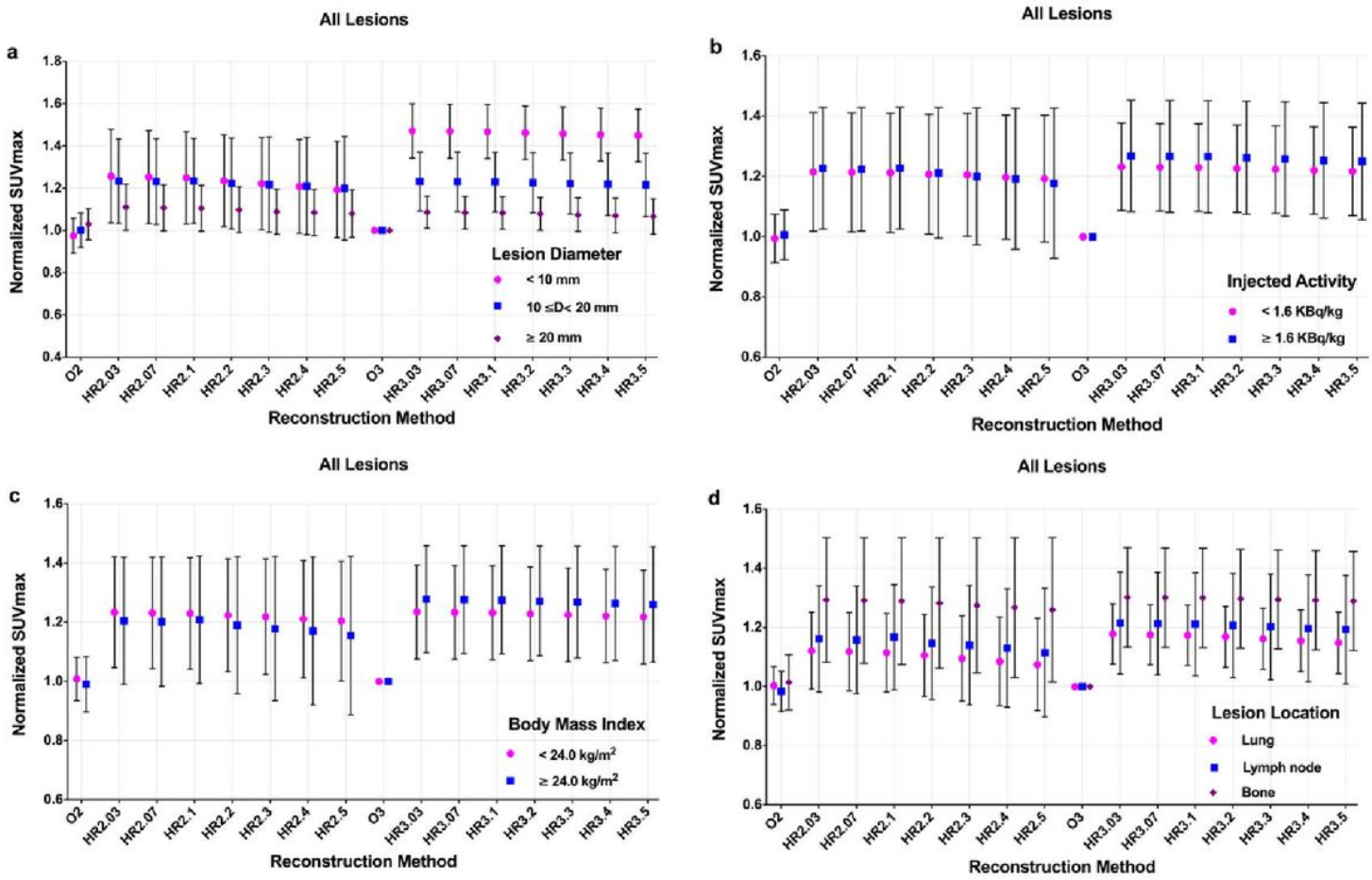

Figure 3

The mean and SD of normalized SUV_{max} for lesions divided by diameter (a), injected activity (b), patient body mass index (c), and location (d) with different reconstruction settings.

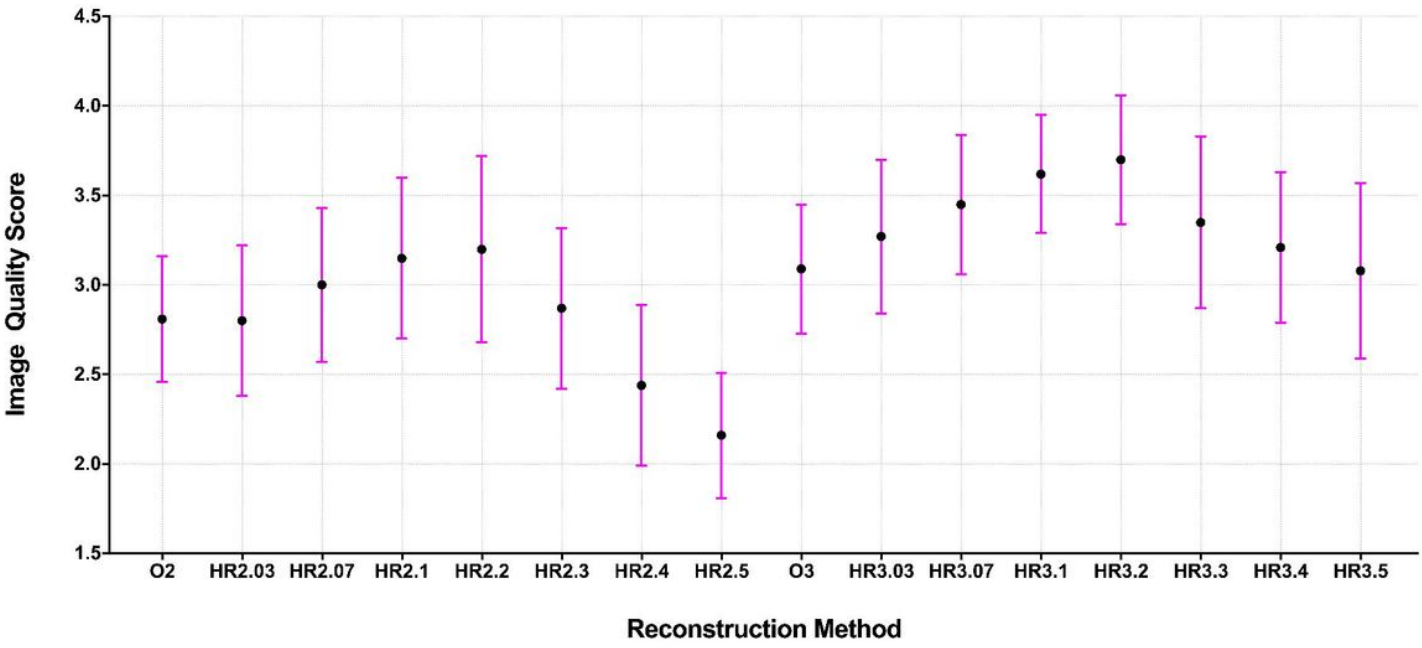

Figure 4

The qualitative image quality score of the clinical images with different reconstruction methods. The mean (filled circle) and standard deviation (error bar) of the image quality scores were plotted for each reconstruction method.

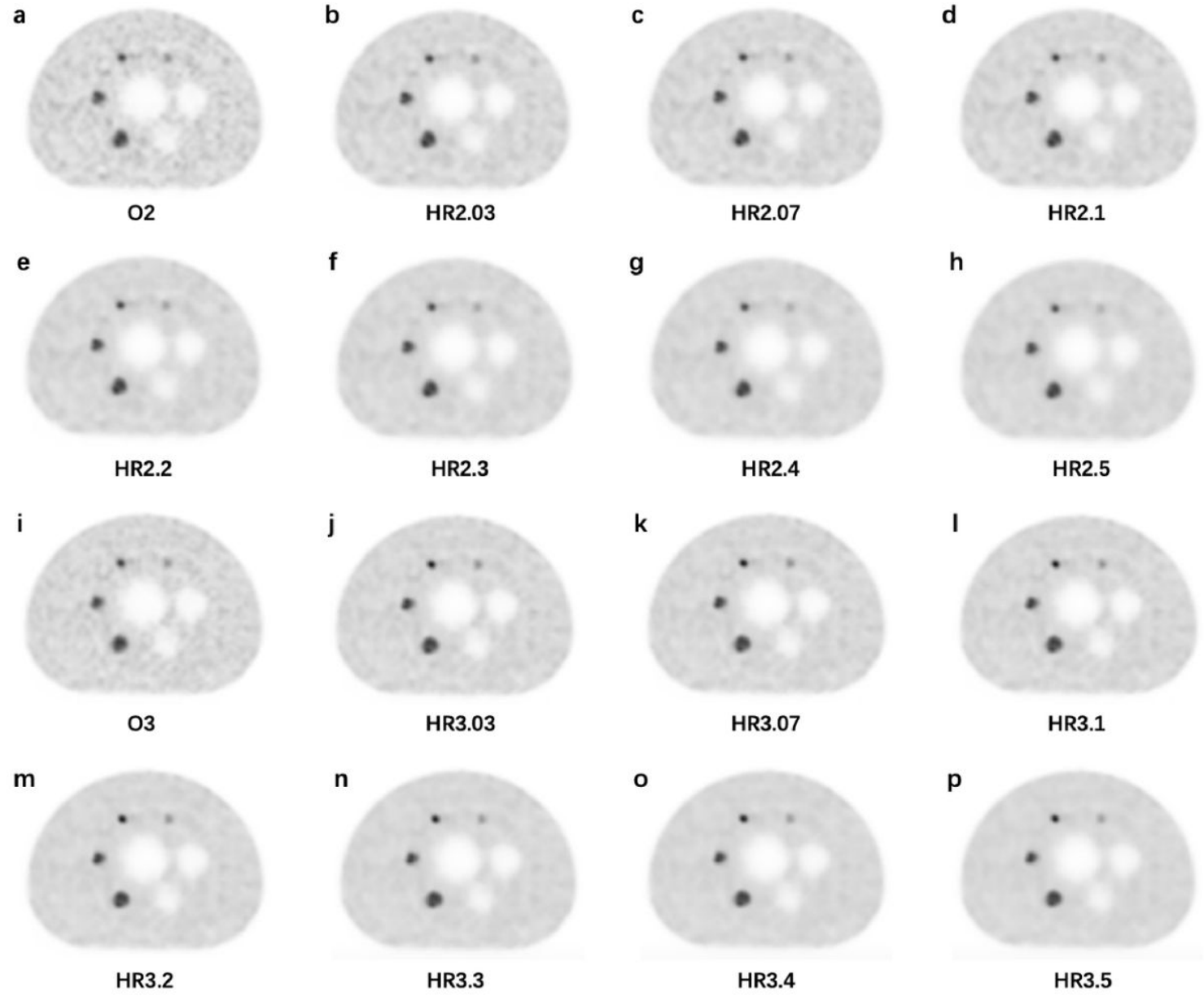

Figure 5

The images for the NEMA phantom with 4 hot spheres filled with ^{68}Ga-DOTA-NOC in a 4:1 contrast ratio. (a) O2, (b) HR2.03, (c) HR2.07, (d) HR2.1, (e) HR2.2, (f) HR2.3, (g) HR2.4, (h) HR2.5, (i) O3, (j) HR3.03, (k) HR3.07, (l) HR3.1, (m) HR3.2, (n) HR3.3, (o) HR3.4, (p) HR3.5.

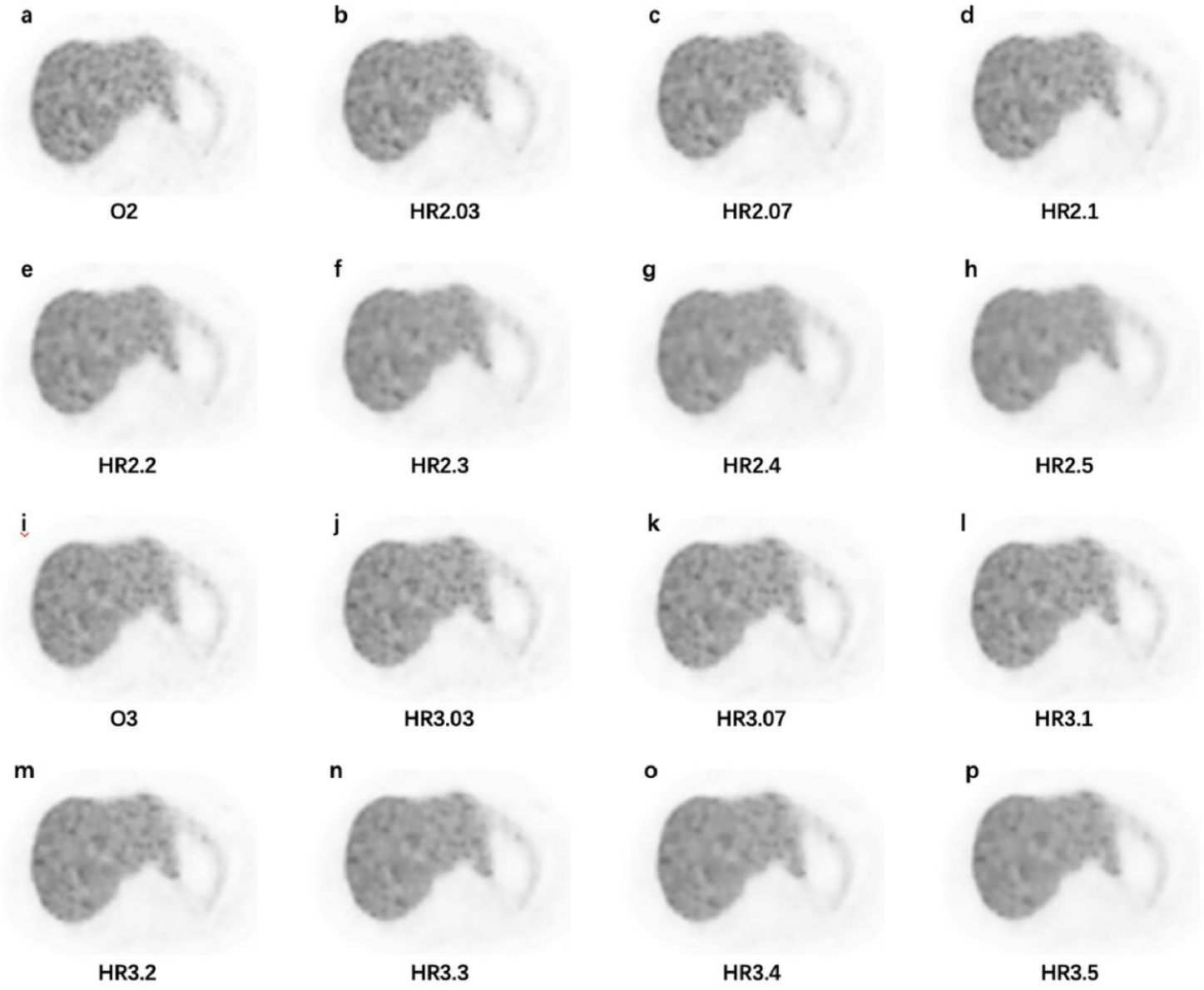

Figure 6

Axial PET images in the liver from a 45-years-old male patient injected 101 MBq ^{68}Ga-DOTA-NOC with adrenal pheochromocytoma for the different reconstruction series (1.68 m, 75 kg, and resting for 50 minutes). (a) O2, CV=13.45; (b) HR2.03, CV=12.73; (c) HR2.07, CV=12.23; (d) HR2.1, CV=11.89; (e) HR2.2, CV=10.91; (f) HR2.3, CV=10.07; (g) HR2.4, CV=9.41; (h) HR2.5, CV=8.74; (i) O3, CV=11.24; (j) HR3.03, CV=11.28; (k) HR3.07, CV=11.11; (l) HR3.1, CV=10.94; (m) HR3.2, CV=10.27; (n) HR3.3, CV=9.76; (o) HR3.4, CV=9.27; (p) HR3.5, CV=8.77.

Figure 7

PET images of a 58-years-old female patient injected with 55.72 MBq ^{68}Ga-DOTA-NOC diagnosed with adrenal pheochromocytoma (1.56 m, 55 kg, and resting for 73 minutes). A lung nodule with low DOTA-NOC uptake is depicted in the images. (a) O2, SUV_{max}=2.23; (b) HR2.03, SUV_{max}=2.99; (c) HR2.07, SUV_{max}=2.88; (d) HR2.1, SUV_{max}=2.80; (e) HR2.2, SUV_{max}=2.49; (f) HR2.3, SUV_{max}=2.16; (g) HR2.4, SUV_{max}=1.8; (h) HR2.5, SUV_{max}=1.46; (i) O3, SUV_{max}=2.31; (j) HR3.03, SUV_{max}=3.43; (k) HR3.07, SUV_{max}=3.36; (l) HR3.1, SUV_{max}=3.37; (m) HR3.2, SUV_{max}=3.18; (n) HR3.3, SUV_{max}=3.01; (o) HR3.4, SUV_{max}=2.81; (p) HR3.5, SUV_{max}=2.57.

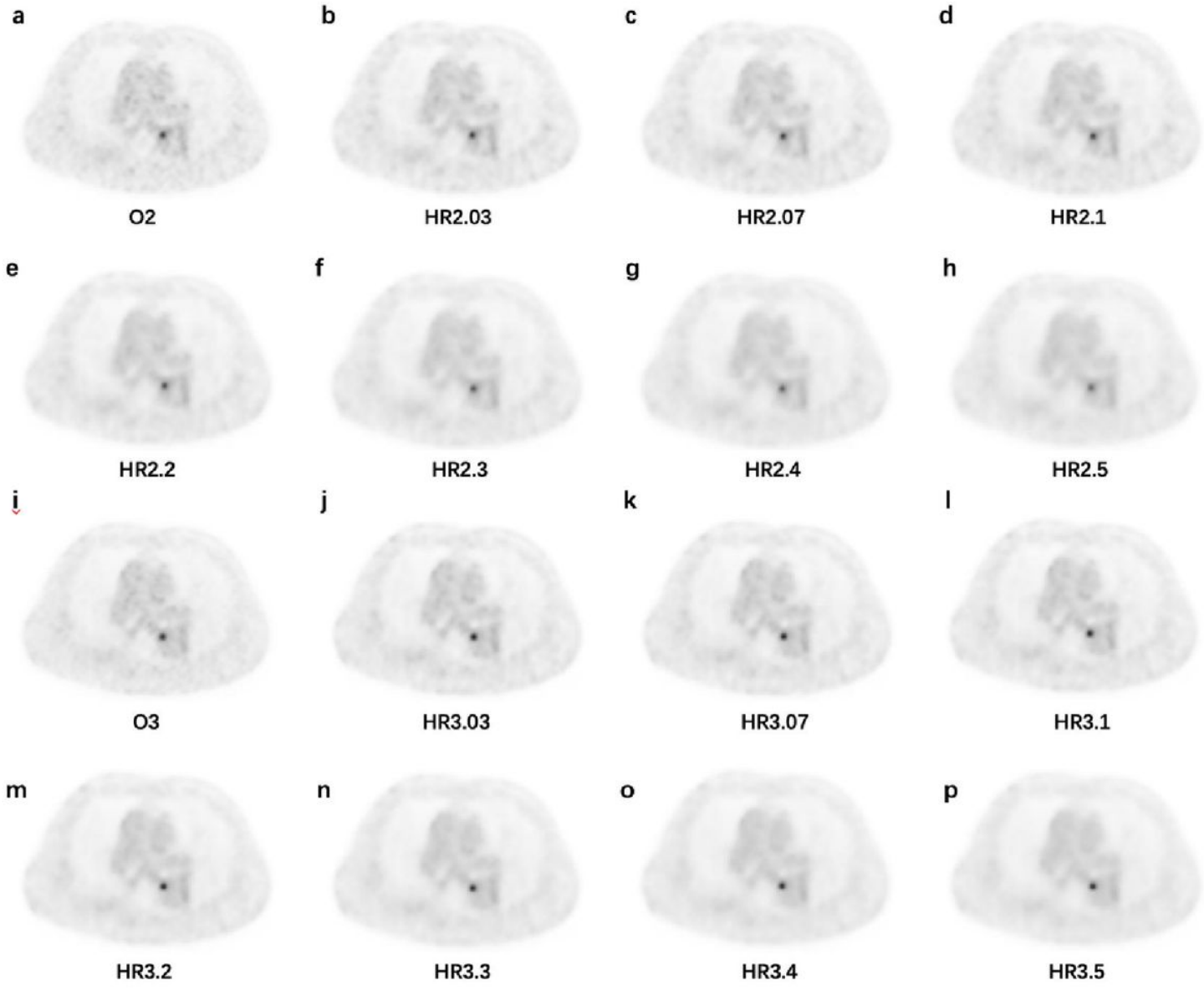

Figure 8

A 79-years-old male patient injected 115.81 MBq ^{68}Ga-DOTA-NOC diagnosed with adrenal pheochromocytoma (1.65 m, 70 kg, and resting for 80 minutes). The images reveal a lymph node with a diameter of 1.13 cm measured on CT image (not shown) and moderate DOTA-NOC uptake. (a) O2, SUV_{max}=6.17; (b) HR2.03, SUV_{max}=6.23; (c) HR2.07, SUV_{max}=6.11; (d) HR2.1, SUV_{max}=6.02; (e) HR2.2, SUV

$_{max}$=5.7; (f) HR2.3, SUV $_{max}$=5.35; (g) HR2.4, SUV $_{max}$=4.90; (h) HR2.5, SUV $_{max}$=4.61; (i) O3, SUV $_{max}$=6.49; (j) HR3.03, SUV $_{max}$=7.11; (k) HR3.07, SUV $_{max}$=7.07; (l) HR3.1, SUV $_{max}$=7.04; (m) HR3.2, SUV $_{max}$=6.93; (n) HR3.3, SUV $_{max}$=6.82; (o) HR3.4, SUV $_{max}$=6.7; (p) HR3.5, SUV $_{max}$=6.58

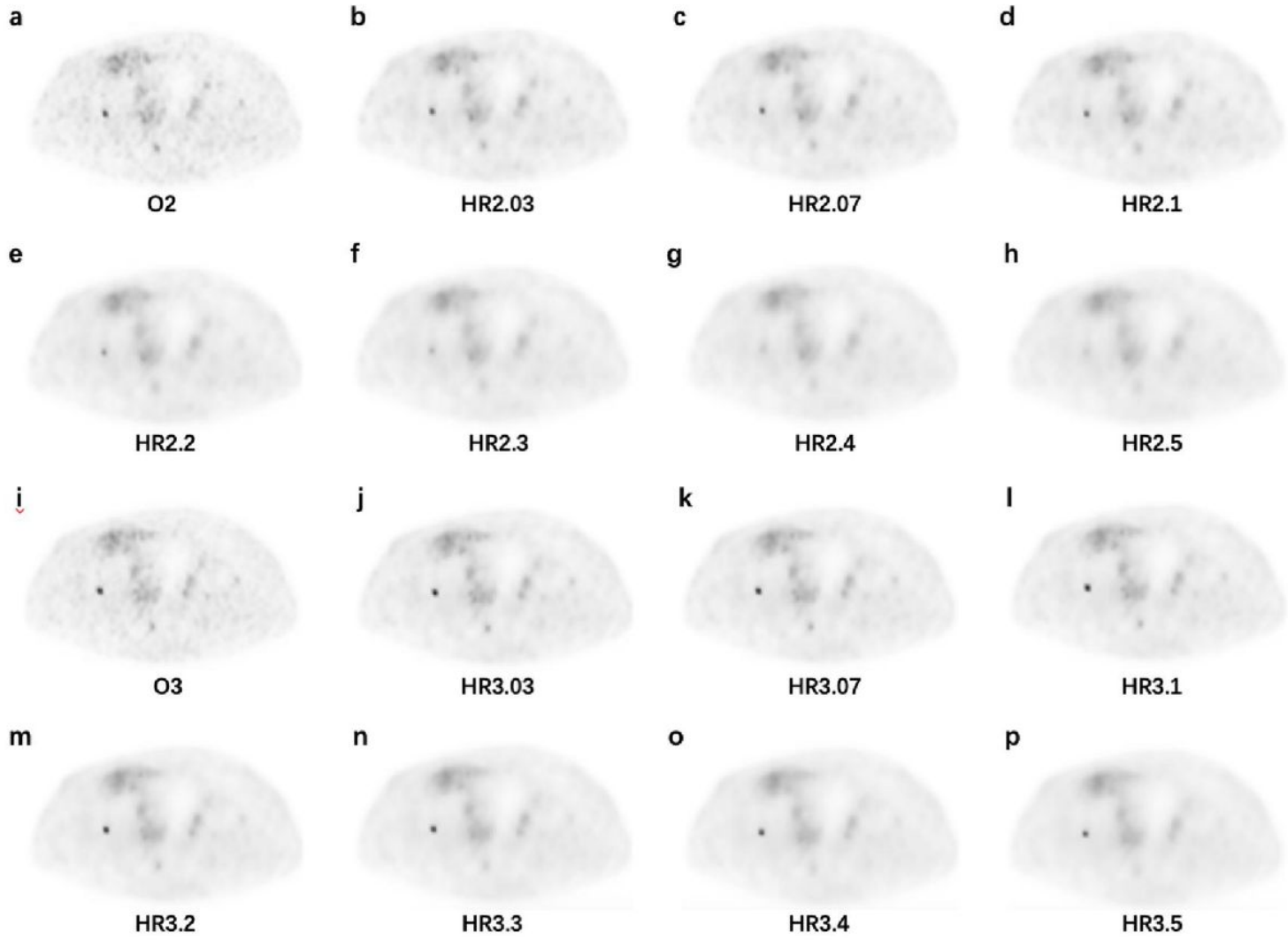

Figure 9

A 69-years-old male patient injected 119.88 MBq ^{68}Ga-DOTA-NOC diagnosed with pancreatic NEN (1.70 m, 60 kg, and resting for 89 minutes). The images demonstrate a small bone lesion with a diameter of 0.88 cm measured on CT image (not shown) and low DOTA-NOC uptake.. (a) O2, SUV $_{max}$=3.82; (b) HR2.03, SUV $_{max}$=3.57; (c) HR2.07, SUV $_{max}$=3.30; (d) HR2.1, SUV $_{max}$=3.07; (e) HR2.2, SUV $_{max}$=2.21; (f) HR2.3, SUV $_{max}$=1.50; (g) HR2.4, SUV $_{max}$=1.16; (h) HR2.5, SUV $_{max}$=1.05; (i) O3, SUV $_{max}$=4.47; (j) HR3.03, SUV $_{max}$=4.72; (k) HR3.07, SUV $_{max}$=4.64; (l) HR3.1, SUV $_{max}$=4.60; (m) HR3.2, SUV $_{max}$=4.41; (n) HR3.3, SUV $_{max}$=4.17; (o) HR3.4, SUV $_{max}$=3.85; (p) HR3.5, SUV $_{max}$=3.44.